

Integration-by-parts reductions of Feynman integrals using Singular and GPI-Space

**Dominik Bendle^{a,b} Janko Böhm^a Wolfram Decker^a Alessandro Georgoudis^c
Franz-Josef Pfreundt^b Mirko Rahn^b Pascal Wasser^d Yang Zhang^{e,f}**

^a*Department of Mathematics, University of Kaiserslautern, 67663 Kaiserslautern, Germany*

^b*Fraunhofer Institute for Industrial Mathematics ITWM, Fraunhofer-Platz 1, 67663 Kaiserslautern, Germany*

^c*Department of Physics and Astronomy, Uppsala University, SE-75108 Uppsala, Sweden*

^d*PRISMA+ Cluster of Excellence, Johannes Gutenberg University, D-55128 Mainz, Germany*

^e*Interdisciplinary Center for Theoretical Study, University of Science and Technology of China, Hefei, Anhui 230026, China*

^f*Max-Planck-Institut für Physik, Werner-Heisenberg-Institut, D-80805 München, Germany*

E-mail: bendle@rhrk.uni-kl.de, boehm@mathematik.uni-kl.de,
Alessandro.Georgoudis@physics.uu.se,
franz-josef.pfreundt@itwm.fhg.de, mirko.rahn@itwm.fhg.de,
wasserp@uni-mainz.de, yzhang@mpp.mpg.de

ABSTRACT: We introduce an algebro-geometrically motivated integration-by-parts (IBP) reduction method for multi-loop and multi-scale Feynman integrals, using a framework for massively parallel computations in computer algebra. This framework combines the computer algebra system SINGULAR with the workflow management system GPI-SPACE, which is being developed at the Fraunhofer Institute for Industrial Mathematics (ITWM). In our approach, the IBP relations are first trimmed by modern algebraic geometry tools and then solved by sparse linear algebra and our new interpolation methods. These steps are efficiently automatized and automatically parallelized by modeling the algorithm in GPI-SPACE using the language of Petri-nets. We demonstrate the potential of our method at the nontrivial example of reducing two-loop five-point nonplanar double-pentagon integrals. We also use GPI-SPACE to convert the basis of IBP reductions, and discuss the possible simplification of IBP coefficients in a uniformly transcendental basis.

KEYWORDS: Scattering Amplitudes, QCD, Computational Algebraic Geometry, Singular, GPI-Space, parallel computations.

Contents

1	Introduction	1
2	Module intersection method reloaded	4
2.1	Module intersection	4
2.2	Linear reduction	6
3	Massively parallel computations using Singular and GPI space	8
4	Parallel matrix reduction as a Petri net	10
4.1	General structure of the algorithm	10
4.2	Managing the interpolation	10
4.3	Description of the Petri net	11
4.4	Parallel timings	14
5	IBP conversion between different integral bases	18
5.1	Dlog basis definition and the dlog algorithm	18
5.2	IBP reduction with a dlog basis	19
6	Two-loop five-point nonplanar double pentagon example	20
6.1	Module intersection with cuts	22
6.2	IBP reduction	23
6.3	IBP coefficients conversion to dlog basis	24
7	Summary	25
A	Rational function interpolation	26

1 Introduction

With the success of Large Hadron Collider (LHC) Run II and the upcoming LHC run III, high precision background computation, especially next-to-next-to-leading-order (NNLO) scattering computation are crucial for the interpretation of experimental results. In recent years, we see great progress have been made in multi-loop scattering amplitude calculations, for instance, the $2 \rightarrow 3$ processes [1–15]. The progress is due to modern developments of scattering amplitudes, like the integrand construction method [16, 17], canonical integrals [18, 19], numeric unitarity [20, 21], bootstrap methods [22–29], finite-field reconstruction [30–32] and new ideas in the integration-by-parts (IBP) reduction. The latter is the main topic to be discussed in this paper.

Frequently, in a computation of scattering amplitudes, IBP reduction is a crucial and bottleneck step. It is a fundamental tool for both the reduction of integrals into master integrals (MI), and for the computation of the master integrals themselves using the differential equation method. IBP identities are derived from an integration of a total derivative [33],

$$0 = \int \frac{d^D \ell_1}{i\pi^{D/2}} \cdots \frac{d^D \ell_L}{i\pi^{D/2}} \sum_{j=1}^L \frac{\partial}{\partial \ell_j^\mu} \frac{v_j^\mu}{D_1^{\nu_1} \cdots D_m^{\nu_m}}, \quad (1.1)$$

where v_j^μ is a polynomial in the loop momenta and the D_i are the inverse propagators.

The standard approach to obtain IBP reductions, by which we are able to express an integral as a linear combination of a finite number of MIs, is to generate a large amount of IBP relations and then use the Laporta algorithm [34] to solve the associated linear system. The algorithm works by imposing an ordering to the different integral families and solving recursively. There exist different both public and private implementations of this approach [35–40]. Usually this approach generates a large linear system to solve.

One possible way to avoid this is to consider a particular set of IBPs which does not have doubled propagators [41–43]. This provides a much smaller linear system. These IBPs without double propagators are physically related to dual conformal symmetries [44]. A further simplification can be made by using unitarity methods, where by considering a spanning set of generating cuts it is possible to reduce the size of the IBP system. This requires the prior knowledge of a basis of MIs. The basis can be obtained by running the Laporta algorithm with constant kinematics or with specified programs such as MINT [45] or AZURITE [46]. (Moreover the dimension of the MIs basis can also be obtained by studying the parametric annihilators [47].) There is also an important technique [48] to nullify all master integrals except one integral, to make the large-scale linear reduction possible.

Beside the advances in purely analytical methods in recent years, there has been a lot of work towards numerical implementations of the IBP identities generation. The idea is to utilize integer values or finite-field values for the kinematical invariants [30, 31, 37], depending on the difficulty of the problem, and then by running the same reduction several times for reconstruction. This method have been very successful in tackling difficult problems. Furthermore, it is possible to numerically solve the IBP relations and skip the IBP coefficient reconstruction to carry out amplitude reconstructions directly. (For examples, see [9, 10, 13, 49]). In this paper we also present our own implementation of a semi-numeric rational interpolation method, see the Appendix A for further details.

Furthermore, new approaches were developed recently to obtain the reduction directly without generating IBP relations from total derivatives. In [50], the direct solution method was presented to derive recurrence relations for Feynman integrals and solve them analytically with arbitrary numerator degree. One very promising progress is based on intersection theory of differential forms from Baikov representation [51–53]. This approach calculates the master integral coefficients from intersection numbers. There is also a very intuitive approach to reduce Feynman integrals by considering the η expansion of the Feynman prescription [54–56]. By this, the reduction computation scales only as the number of master

integrals. Furthermore, it is possible to determine two-loop planar diagram IBP coefficients directly from the Baikov representation [57].

In this paper, we present our new powerful IBP reduction method based on

1. Computational algebraic geometry. We apply the module intersection method [58, 59] as well as the degree bound on the Gröbner basis computation, to efficiently generate a small IBP system, without double propagators (or IBPs with a limit on the propagator power).
2. The modern framework of massively parallel computations in computer algebra, which combines the computer algebra system SINGULAR [60] with the workflow management system GPI-SPACE [61]. We have completely automatized our approach and make our algorithms run automatically in parallel on high performance computing clusters. In this way, IBP results can be obtained in an efficient, reliable and scalable way. From example, our implementation can automatically determine the number of points needed for an interpolation, identify possible “bad” points, add more points, and interpolate the final result.

We demonstrate the power of our method by reducing the two-loop five-point nonplanar double pentagon diagram *analytically*, up to the numerator degree 4. This is a nontrivial test since the diagram has a complicated topology and there are five symbolic Mandelstam variables as well as the spacetime variable D .

Furthermore, we start to look at the possible simplification of IBP coefficients by converting the master integral basis. In this paper, we tested the conversion to the “dlog” basis [62], a special case of the canonical basis [19]. We find that that with the dlog basis, in this example, the IBP coefficients size of our target integrals reduces significantly by 76%, i.e. from the byte size $\sim 2.0\text{G}$ in the Laporta basis to $\sim 0.48\text{G}$ in the dlog basis on disk. The master integral basis conversion computation is also automated by our SINGULAR and GPI-SPACE program.

The paper is structured as follows: in Section 2 we present the general background on how to generate simple and trimmed IBP systems using computational algebraic geometry and finite-field methods, as well as the improvement on the algorithm in [58]. In Section 3 we give a short overview on how we use SINGULAR in conjunction with GPI-SPACE. In Section 4, we describe how to model our algorithm in the SINGULAR-GPI-SPACE framework. This, in particular, demonstrates the general potential of the SINGULAR-GPI-SPACE framework for applications in high-energy physics. In Section 5 we review the algorithmic computation of a dlog basis, which has uniform transcendental weight, and we comment on how to convert coefficients from the Laporta basis to the dlog basis. In Section 6 we present a working example of our implementation, the double pentagon graph. We discuss the analytic IBP reduction and the conversion of IBP coefficients to the dlog basis. Finally we present a summary and conclusion of this paper.

The result of our IBP reductions can be downloaded from the following links:

https://www.dropbox.com/s/1ubdhcyhe8e4pwy/IBPmatrix_Laporta_basis.tar.gz

has the IBP coefficients in the Laporta basis with the scale $s_{12} = 1$.

https://www.dropbox.com/s/e6t4evftkfo95pr/IBPmatrix_dlog_basis.tar.gz

contains the IBP coefficients in the dlog basis with the scale $s_{12} = 1$. For the convenience of readers, we also upload the IBP coefficients in the dlog basis with the full scale dependence,

https://www.dropbox.com/s/dnkr6h5t3vik2r0/IBPmatrix_dlog_basis_scaled.tar.gz

We encourage researchers in high energy community to send us IBP reduction problems (mailto: alessandro.georgoudis@physics.uu.se), for cutting-edge precision calculations and further sharpening our new reduction method.

2 Module intersection method reloaded

In this section, we present a refined version of the approach of using module intersection to trim IBP systems. For the detailed account on the module intersection IBP reduction method, we refer to [58].

2.1 Module intersection

The Feynman integrals under consideration are labeled as,

$$I[n_1, \dots, n_m] = \int \frac{d^D l_1}{i\pi^{D/2}} \cdots \frac{d^D l_L}{i\pi^{D/2}} \frac{1}{D_1^{n_1} \cdots D_m^{n_m}}. \quad (2.1)$$

where L is the loop order and l_i 's are the loop momenta. We have E independent external vectors that we label as p_1, \dots, p_E . We assume that the Feynman integrals have been reduced on the integrand level, and set $m = LE + L(L + 1)/2$ which equals the number of scalar products in the configuration.

We find that it is convenient to use the Baikov representation [45, 63] for IBP reductions,

$$I[n_1, \dots, n_m] = C_E^L U^{\frac{E-D+1}{2}} \int dz_1 \cdots dz_m P^{\frac{D-L-E-1}{2}} \frac{1}{z_1^{n_1} \cdots z_m^{n_m}}, \quad (2.2)$$

where P is the Baikov polynomial, which can be written as a Gram determinant:

$$P = \det G \begin{pmatrix} l_1, \dots, l_L, p_1, \dots, p_E \\ l_1, \dots, l_L, p_1, \dots, p_E \end{pmatrix}, \quad (2.3)$$

U is another Gram determinant, and C_E^L is a constant factor

$$U = \det G \begin{pmatrix} p_1, \dots, p_E \\ p_1, \dots, p_E \end{pmatrix}, \quad C_E^L = J \frac{\pi^{\frac{L-m}{2}}}{\Gamma(\frac{d-E-L+1}{2}) \cdots \Gamma(\frac{d-E}{2})}, \quad (2.4)$$

where J is a constant Jacobian. The factors U and C_E^L are irrelevant for the IBP relations.

As in [20, 43, 64], the IBP relations in Baikov representation read,

$$0 = \int dz_1 \cdots dz_m \sum_{i=1}^m \frac{\partial}{\partial z_i} \left(a_i(z) P^{\frac{D-L-E-1}{2}} \frac{1}{z_1^{n_1} \cdots z_m^{n_m}} \right), \quad (2.5)$$

where each $a_i(z)$ is a polynomial in the variables z_i . Note that P vanishes on the boundary of the Baikov integration domain, so this form of IBP identities does not have surface terms.

Suppose that the goal is to reduce the integral family with $n_j \leq 0$, $j = k + 1, \dots, n$, i.e., integrals with the propagators $1/(D_1 \dots D_k)$ and the sub-topology integrals. We use the idea of considering IBP systems without double propagators [41] and choose suitable $a_i(z)$ to prevent the appearance of double propagators in (2.5). In Baikov representation, we also need to prevent total derivatives with dimension shifts [20, 43]. These constraint translates into the following syzygy equations

$$\left(\sum_{i=1}^m a_i(z) \frac{\partial P}{\partial z_i} \right) + bP = 0, \quad (2.6)$$

$$a_i(z) = b_i(z)z_i, \quad i = 1, \dots, k. \quad (2.7)$$

where $b(z)$ and $b_i(z)$ are also polynomials in z_i 's. Relation (2.6) avoids dimension shifts of the integrals, while (2.7) ensures that there is no double propagator for D_i if the initial index $n_i = 1$ in (2.5). The goal is to find such polynomials $a_i(z)$, $b(z)$ and $b_i(z)$. Since we require polynomial solutions, this is not a linear algebra problem, but a computational algebraic geometry problem.

We use the module intersection method from [58, 65] to solve (2.6) and (2.7) simultaneously. Note that the analytic generators of all solutions of (2.6) can be directly written down via either the canonical IBP vector method [20] or the Gram matrix Laplace expansion method [59]¹. The relations in (2.7) can be trivially expressed as a module membership condition. Hence without any algorithmic computation, we know the individual solutions for (2.6) and (2.7). These form polynomial sub-modules of R^n over the polynomial ring $R = \mathbb{Q}(c_1, \dots, c_t)[z_1, \dots, z_m]$ (where c_1, \dots, c_t are Mandelstam variables and mass parameters). We denote these modules in the following as M_1 and M_2 , respectively. The task is then to compute

$$M_1 \cap M_2. \quad (2.8)$$

This module intersection can be obtained by computing a module Gröbner basis in a particular ordering [58]. One decisive strategy is the *localization* technique, which is to compute $M_1 \cap M_2$ over the polynomial ring $\tilde{R} = \mathbb{Q}[c_1, \dots, c_t, z_1, \dots, z_m]$. In this manner, we treat kinematic variables equal to the Baikov variables. This greatly speeds up the intersection computation for multi-scale problems, but results in a redundant generating system. The latter can be trimmed further by importing the result back to R^m and removing redundant generators by checking the leading monomials. This is powered by SINGULAR's command **simplify**. Once $M_1 \cap M_2$ is obtained, we know all simultaneous solutions for (2.6) and (2.7), and use (2.5) to get IBPs without doubled propagators.

We emphasize that, although (2.6) and (2.7) were originally designed for IBPs without doubled propagators, the solutions of (2.6) and (2.7) can be used to simplify IBP systems

¹We learned the Laplace expansion method from Roman Lee, and proved its completeness via the Gulliksen-Negard / Jozefiak exact sequence in [59].

with double or multiple propagators. Using these solutions $a_i(z)$, the resulting IBP system does not introduce integrals with higher powers of propagators, and hence also greatly decreases the size of the IBP system.

Frequently, instead of computing IBPs directly, we compute IBPs on spanning cuts and assemble the full IBPs afterwards. This amounts to setting some of z_i to zero in (2.6) and (2.7). We refer for details on cut IBPs in Baikov representations to [58].

Compared to the approach in [58], we present the following new features of the module intersection method in this paper:

- When we compute the intersection $M_1 \cap M_2$, instead of finding a full generating system, we heuristically impose a polynomial degree bound in the computation. Then we reduce the resulting IBPs over finite fields to test if we already get all the IBP relations needed. If the IBP relations are insufficient, we increase the degree bound and repeat the computation. This approach speeds up the intersection computation dramatically in many cases. In practice, we use the option **degbound** in the computer algebra software SINGULAR to set the degree bound.
- In the approach of [58], the module intersection was only computed for the top sector, and it is sufficient to reduce integrals to a master integral basis. However, in this paper, we compute the module intersection for the top sector and also all sub-sectors, which seems to generate more IBP relations. By the linear algebra trimming discussed in the next subsection, this approach eventually gives a block triangular linear system and makes the linear reduction easier.

2.2 Linear reduction

For the simplified IBP system arising from the module-intersection method, we then use our own linear reduction algorithm to reduce the IBP system. The steps are:

1. Trimming of the linear system from the module intersection method. We do this in two stages: (a) Set all the kinematic variables to integer values, and use linear algebra over a finite field to find the independent IBP relations. (b) Again over a finite field, carry out the reduction. From the intermediate steps, we can determine a sufficient subset of IBP relations for reducing the target integrals. These operations are powered by the finite field computation tool SPASM[66].
2. Remove the overlap between two different cuts and simplify the linear system: If two cuts have a common master integral, we use the idea from [48], to set the master integral to zero in one of the two cut IBP systems. This will later on dramatically simplify the IBP reduction for the cut.
3. For the linear system simplified by the first two steps, we use our own SINGULAR row reduce echelon form (RREF) code over function fields to reduce the target integrals to master integrals. Our code applies both row and column swaps for finding the optimal pivots. Note that column swaps would change the set of master integrals. After the RREF computation, we convert the new master integrals to the original

master integrals. We have observed that this approach is in general much faster than fixing the column ordering and directly reducing the target integrals to the original master integrals.

For difficult IBP reduction computations, we use a “semi-numeric” approach: This approach sets several but usually not all of the kinematic variables for the reduction computation to numeric values (i.e., to constant integers). Without loss of generality, for the kinematic variables (c_1, \dots, c_k) , we set

$$c_i \mapsto a_i, \quad a_i \in \mathbb{Z}, \quad 1 \leq i \leq k_1 \quad (2.9)$$

where $k_1 < k$.

The actual degree of the coefficients in these variables can be decided by a univariate analytic computation (that is we set all but one of the c_i to constant values). For example, we set the dimension D and all parameters c_i except c_1 as random integers, and then carry out the reduction. This computation is much easier than the actual IBP reduction with fully analytic parameters. From the reduction, we determine the degree of c_1 in the final IBP reduction coefficients. From the degrees of the c_i , we determine the minimal number of semi-numeric points for the subsequent interpolation step. (See [31] for an alternative way of finding the degree of each parameters in a rational function.)

After accumulating enough points, we collect the semi numeric reduction results and interpolate to get the final IBP reduction coefficients. To do this, we first run step 3 for a semi-numeric set of parameters, find the optimal pivots and record the row/column swap history as a *trace* of our computation. For other numeric values, we always use the same trace to ensure the relatively uniform running time of the computation.

In practice, we use our rational function interpolation algorithm described in Appendix A. We carefully choose one “reference” semi-numeric point,

$$c_j \mapsto b_j, \quad b_j \in \mathbb{Z}, \quad k_1 < j \leq k \quad (2.10)$$

and keep c_1, \dots, c_{k_1} symbolic to do a reduction computation. Using the reference point result, we convert the rational function interpolation problem to separate polynomial interpolation problems for numerators and denominators. By this algorithm, the number of “semi-numeric” computations is,

$$(d_1 + 1) \times (d_2 + 1) \times \dots \times (d_{k_1} + 1) \quad (2.11)$$

where d_i , where $1 \leq i \leq k_1$. Here d_i is the maximal degree of c_i in the numerator and denominator polynomials in the RREF matrix. This algorithm is also implemented in SINGULAR.

For the semi-numerical reduction and interpolation, we need to parallelize our computation in an efficient way. Furthermore, with semi-numeric points, we may have some bad points in the reduction or interpolation. In order to make use of massively parallel computations in an efficient way, and to make the bad points replacement workflow automatic, we use the modern workflow management system GPI-SPACE, which is being developed by Fraunhofer ITWM, in conjunction with the computer algebra system SINGULAR. We will discuss the ideas behind this approach in the subsequent section.

3 Massively parallel computations using Singular and GPI space

Large scale calculations, for example, row reductions of integration-by-parts identities in the case of interesting Feynman diagrams, are only possible due to use of parallel computing on high-performance clusters. The use of modern computer algebra methods requires to model complicated algorithms, which rely on sub-computations with time and memory requirements that are difficult to predict a priori. This is, for example, due to the use of Buchberger’s Algorithm for finding a Gröbner basis or, more generally, due to the explosion of the size of expressions in polynomial computations. As a result, while in the context of numerical simulations massively parallel methods are nowadays a standard tool, these methods are only recently taking a center stage in symbolic computations [67, 68]. In order to support the general use of parallel methods in advanced algorithms in computer algebra, there is an ongoing effort to join the computer algebra system SINGULAR for polynomial calculations with the workflow management GPI-SPACE [61]. GPI-SPACE consists of a scheduler distributing the actual computations to workers in the cluster, a virtual memory layer to facilitate communication between the workers, and a workflow management system, which makes use of a model of the algorithm under consideration in terms of a so-called Petri net.

A Petri net is a directed bipartite graph with two kinds of nodes: *places* which can hold a number of indistinguishable *tokens*, and *transitions*, which consume one token from each input place and put one token on each output place. Transitions can only operate (we say they are enabled) if on each input place there is at least one token available (see Figure 1 for an enabled transition and its firing, and Figure 2 for a transition, which is not enabled). In the figures, places are shown as circles, transitions as rectangles, and tokens as black dots.

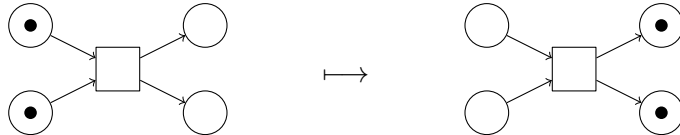


Figure 1. Enabled transition and it’s firing.

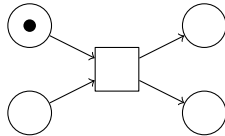


Figure 2. Transition which is not enabled.

A Petri net is executed by iteratively firing random enabled transitions. We have observed that this randomized reformulation can make various algorithms in computer algebra

behave much more consistently and predictably throughout the course of the computation than their deterministic counterparts.

While the coarse-grained structure of the algorithm is modeled in terms of a Petri net, the transitions will call procedures from the C-library version SINGULAR to do the actual computations. In fact, any library with a C-interface can be used in this way. The result of this setup is a flexible framework for massively parallel computations in computer algebra. This framework has, for example, already been used to implement a non-singularity test for algebraic varieties [67, 69], the computation of combinatorial objects in geometric invariant theory [70], and the computation of tropical varieties associated to algebraic varieties [71].

For efficient use in practical programming, the abstract concept of a Petri net has to be extended. Hence, GPI-SPACE provides multiple additional features which go beyond the pure notion of a Petri net:

- Modeling of complicated algorithms just by the use of structure-less tokens is not very efficient. In GPI-SPACE tokens can have a data type and hold actual data. In fact, it is often more efficient to store in a token only a reference to a storage place for the data (in memory or in the file system). By making use of the memory manager of GPI-SPACE or the powerful file systems in modern high-performance cluster, computations can then scale far beyond the limitations of a single machine.
- Transitions can impose conditions on the input tokens in order to fire.
- Transitions in practice involve computations, which take time. Due to the properties of Petri nets, this allows us to execute different transitions, provided they are activated, at the same time (task parallelism) and to execute multiple instances of the same transition in parallel, provided the input places hold multiple tokens (data parallelism). In Figure 3, the transitions f_1 and f_2 can fire in parallel, and, if the input place of f_i holds multiple tokens, then f_i can fire in multiple instances.

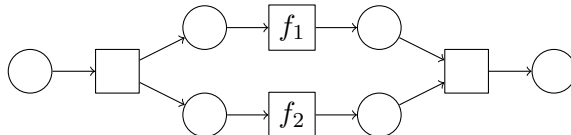


Figure 3. Parallelism in a Petri net.

We have observed that some algorithms in computer algebra run significantly faster and scale in a superlinear way, when implemented in parallel as a Petri net, since they can automatically determine at runtime from multiple possible paths to the solution that one which leads to the solution in the fastest possible way (see [67, Section 6.2]).

In the next section, we illustrate the use of the SINGULAR-GPI-SPACE framework for applications in high-energy physics by modeling our IBP reduction algorithm.

4 Parallel matrix reduction as a Petri net

4.1 General structure of the algorithm

In order to show the practical use and the significant potential of the SINGULAR-GPI-SPACE framework for algorithmic problems arising from high-energy physics, we describe in this section how to model the parallel IBP reduction algorithm in terms of a Petri net. This includes a massively parallel execution of row-reductions over function fields, where a number of parameters has been replaced by integers, and a parallel interpolation step to reconstruct the dependency on these parameters.

So the task is to find the reduced row-echelon form M_{red} of a large linear system of equations, given as a matrix M over the rational function field $\mathbb{Q}(c_1, \dots, c_\ell)$. Since applying Gaussian elimination directly is not feasible, we instead substitute some parameters, say the first r ones, by the coordinates of a point $a \in \mathbb{Z}^r$ and then compute the reduction

$$(M|_{c_1 \rightarrow a_1, \dots, c_r \rightarrow a_r})_{\text{red}}.$$

Details on the algorithm handling this reduction step are given in Section 2.2. To determine the required number of interpolation points a needed to reconstruct the dependency on c_1, \dots, c_r , we find bounds for the degrees of numerators and denominators for each parameter by doing a univariate row reduction (that is, with all but one parameter set to be numeric). After the reduction, we check that the resulting matrix is equal to the desired result

$$M_{\text{red}}|_{c_1 \rightarrow a_1, \dots, c_r \rightarrow a_r}.$$

by normalizing it relative to a previously computed reference matrix with c_{r+1}, \dots, c_ℓ constant and performing degree checks using the exact degrees obtained from the univariate calculations. These steps are described in more detail in Appendix A. Finally, the reduced matrices are then iteratively combined by univariate interpolation (see Appendix A) to produce the final result M_{red} .

Let d_1, \dots, d_r be degree bounds for the entries of M_{red} in the parameters c_1, \dots, c_r , respectively. To obtain M_{red} by interpolation, we need $d_1 + 1$ matrices over $\mathbb{Q}(c_2, \dots, c_\ell)$ of the form

$$M_{\text{red}}|_{c_1 \rightarrow a_1^{(0)}, \dots, M_{\text{red}}|_{c_1 \rightarrow a_1^{(d_1)}} \quad (4.1)$$

for $d_1 + 1$ values $a_1^{(0)}, \dots, a_1^{(d_1)} \in \mathbb{Z}$. Similarly, to obtain any one of the above matrices, we require $d_2 + 1$ matrices over $\mathbb{Q}(c_3, \dots, c_\ell)$ and so on, until this process ends at the matrices over $\mathbb{Q}(c_{r+1}, \dots, c_\ell)$ which are computed by substitution of c_1, \dots, c_r and subsequent reduction. This tree-like dependency structure is depicted in Figure 4.

4.2 Managing the interpolation

We model the current status of the interpolation process in a tree structure, which contains at the leaves references to the reduction results, and at its nodes references to the interpolation results. According to this data structure reductions and interpolations are executed within GPI-SPACE. The tree is generated as soon as the degree bounds d_1, \dots, d_r

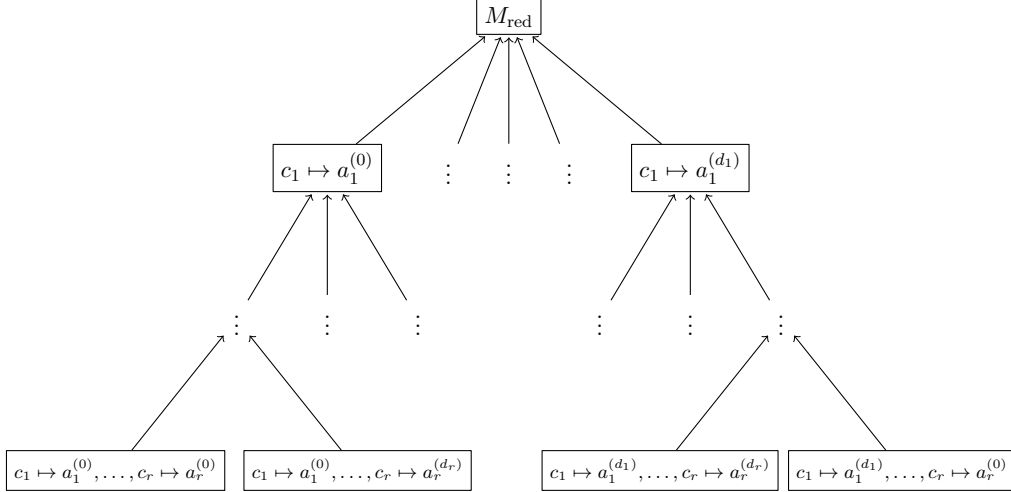


Figure 4. Structure of the interpolation tree

are known, and is extended if the algorithm requires additional data points in case of occurrence of bad interpolation points.

4.3 Description of the Petri net

Figure 5 depicts the Petri net that implements the complete reduction algorithm. In addition to the standard syntax introduced in Section 3, the black dot indicates the initial (structureless) token to get the net started. Moreover, dashed arrows stand for read-only access, i.e. the data in a place is not consumed. The dotted arrows illustrate read and write access to the interpolation tree described in Section 4.2. Transitions can be annotated by conditions, which indicate that the transition can only fire for input tokens for which the condition evaluates to true.² In the following, we describe the individual structures of the net:

Input tokens: The net is initialized with two tokens: A structureless control-token which enables `init` or `trace`, and the input data token on the place `I`, which holds the following data:

- The input linear relations, which are given as a matrix M over the rational function field $\mathbb{Q}(c_1, \dots, c_\ell)$.
- The vector of indices of the parameters which will be interpolated (in the following we assume these indices are $1, \dots, r$).
- The vector of indices of the target variables.
- **Optionally:** A precomputed trace for the reduction step (consistent with the targets). In the net, the trace is referred to as `I.trace` using the usual dot-notation for sub-data structures. Note that the trace fixes the master variables.

²In conditions the name of the place and a token on the place are used interchangeably.

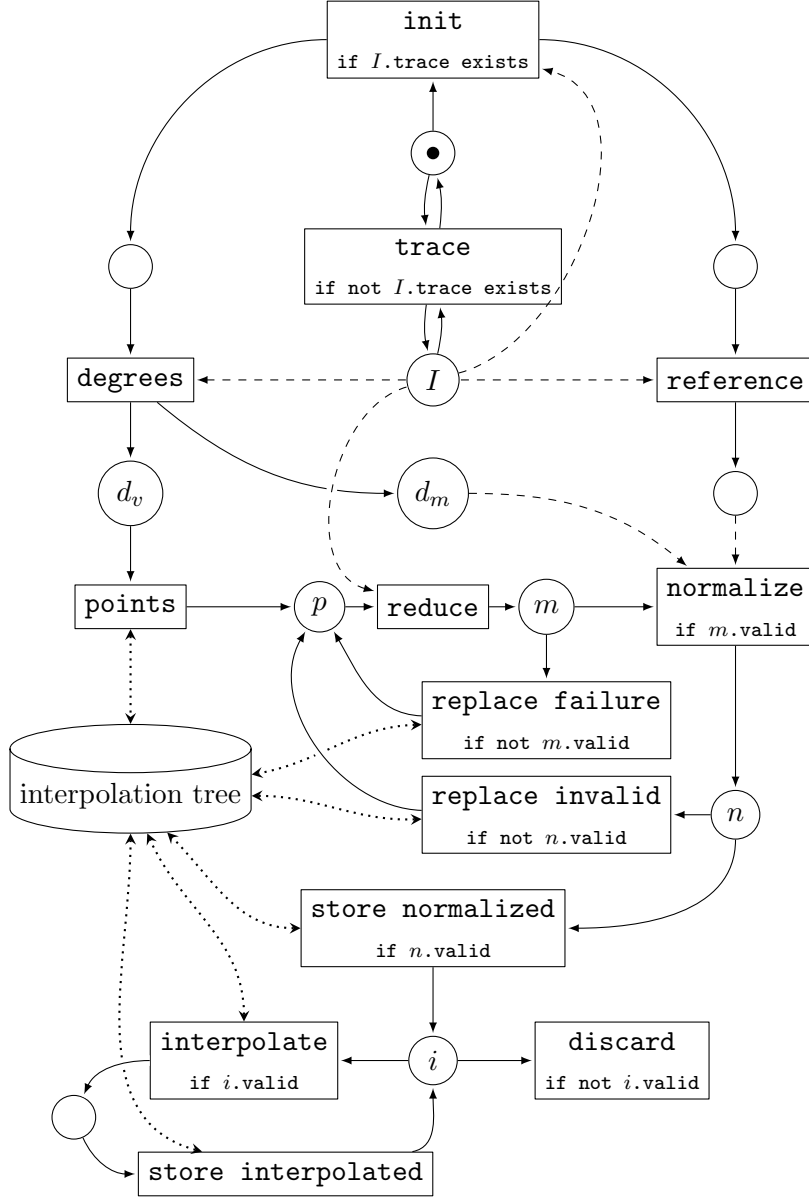


Figure 5. Petri net for row reduction via interpolation. A description of the syntax is given in the first paragraph of Section 4.3

Transition trace: If the token in I does not contain a trace, then **trace** is enabled, computes a trace for the linear reduction (see Section 2.2), adds it to the data token in I .

Transition init: If the input token in I contains trace data, **init** is enabled, fires and produces on each of its output places a structure-less control token to enable the transitions **degrees** and **reference**.

Transition reference: This generates a random substitution point $q = (q_{m+1}, \dots, q_n)$ with values for all parameters which will *not* be interpolated, substitutes these values and

runs the row reduction step (see Section 2.2), that is, computes

$$M_{\text{ref}} := (M|_{c_{r+1} \mapsto q_{r+1}, \dots, c_{\ell} \mapsto q_{\ell}})_{\text{red}}.$$

It stores the actual result in the file-system for later access and produces an output token which contains a reference to the result as well as q . This data will be used later in the normalization step of the interpolation (see above).

Transition degree: This generates a substitution point $p^{(j)} \in \mathbb{Z}^{\{1, \dots, j-1, j+1, \dots, \ell\}}$ for each $1 \leq j \leq \ell$ which yields a matrix

$$M^{(j)} := M|_{c_1 \mapsto p_1^{(j)}, \dots, c_{j-1} \mapsto p_{j-1}^{(j)}, c_{j+1} \mapsto p_{j+1}^{(j)}, \dots, c_{\ell} \mapsto p_{\ell}^{(j)}}$$

over the field $\mathbb{Q}(c_j)$. After applying the row reduction, $M_{\text{red}}^{(j)}$ can be used to determine degree bounds for the parameter c_j for each entry of the final result M_{red} .

For $j \leq r$, we need a global degree bound to determine the number of interpolation points. We thus take the maximum of all numerator and denominator degrees of entries of $M_{\text{red}}^{(j)}$, and store these in a vector in $\mathbb{N}_0^{\{1, \dots, r\}}$, which is put on the place d_v .

If $j > r$, two integer matrices will be produced, which store the degrees of the numerators and denominators of each entry of M_{red} , respectively. This information will be used later to filter out bad interpolation points where polynomial cancellation occurs (see Section A). The result is stored in the file system and a token with a reference to the result is put on the place d_m .

Note, that **degree** is in fact modeled by a sub-Petri net, which behaves in a hierarchical manner as a transition. In practice, we actually compute multiple matrices $M^{(j)}$ per parameter to reduce the probability of a bad point producing wrong degree bounds.

Transition points: This transition takes the degree data in d_v and initializes the interpolation tree, which is described in Section 4.2 and depicted in Figure 4. This, in turn, produces the corresponding set of interpolation points, which are put as separate tokens on the place p .

Transition reduce: This transition consumes a point $p' \in \mathbb{Z}^{\{1, \dots, r\}}$ from the place p and computes

$$(M_{c_1 \mapsto p'_1, \dots, c_m \mapsto p'_r})|_{\text{red}}.$$

The resulting matrix together with its interpolation point are put to on the place m . Since **reduce** performs parameter substitution in rational function expression, the computation may fail due to division by zero. If this happens, $m.\text{valid}$ is set to **false**, **true** otherwise.

Transition replace failure: If for an input token $m.\text{valid}$ is **false**, the token is consumed by the transition **replace failure**, which marks the respective interpolation point as failed in the interpolation tree. If necessary, the interpolation tree is extended by additional interpolation points, which are also put on the place p .

Transition normalize: If for an input token m .valid is true, then m is consumed by `normalize`. This transition reads M_{ref} and fits the input matrix referenced by m with a suitable constant factor. It also compares the entries with the degree matrices in d_m to identify bad interpolation points. The result is put on the place n . If the corresponding point was bad, n .valid is set to `false`, otherwise to `true`.

Transition replace invalid: If for an input token n .valid is false, then the transition `replace invalid` generates new interpolation points in a similar fashion as in `replace failure`.

Transition store normalized: If n .valid is true, this transition marks the corresponding interpolation point as successful in the external storage. If enough interpolation points for a given parameter are finished successfully, the storage produces a token for the respective interpolation which is put on the place i . If the point (p'_1, \dots, p'_r) triggers the interpolation (which will then use further points of the form $(p'_1, \dots, p'_{r-1}, p''_r)$), the result of the interpolation will be associated to the point (p'_1, \dots, p'_{r-1}) in the interpolation tree. If there are not yet enough interpolation points, the transition produces a token which only contains i .valid with value `false`.

Transition discard: This transition discards tokens with i .valid equal to `false`.

Transition interpolate: Tokens with i .valid equal to `true` are consumed by this transition, which then retrieves the references to the input data for the interpolation from the interpolation tree, loads the respective data from the file system, and executes the interpolation. If (in the above notation) the token holds (p'_1, \dots, p'_{r-1}) , then for $(d_v)_r + 1$ many points the corresponding row reduced matrices are retrieved from the storage. Note that due to the tree structure of the interpolation tree, all these points must have the first $r - 1$ coordinates equal to (p'_1, \dots, p'_{r-1}) . The interpolation is then performed entry-wise as explained in Section A.

Transition store interpolated: This transition marks the current point (p'_1, \dots, p'_{r-1}) in the interpolation tree as finished. If $r > 1$ s just like in `store normalized`, the transition produces an interpolation token for the next parameter. If $r = 1$, we have arrived at the final result, and a token with i .valid equal to `false` is produced, which will be discarded. The Petri net contains additional infrastructure (not described here), which terminates the execution once no tokens exist any more on the places i and p .

4.4 Parallel timings

In this section we illustrate the efficiency of our parallel algorithm from Section 4.3. We use the cut $\{1, 3, 4, 5\}$ of the double pentagon diagram, which is discussed in detail in Section 6. This cut is one of the easier ones that have to be considered for this example. We choose this example, since it allows us to finish the computation also on small number of cores, which is necessary to analyze the scaling of our algorithm. In Table 1 we give timings for different numbers of cores used in our algorithm. The computations were performed on the high performance compute cluster at the Fraunhofer Institute for Industrial Mathematics

(ITWM). Each compute node provides two Xeon E5-2670 processors, which amounts to 16 cores³ running at a base clock speed of 2.6 GHz. Each node has 64 GB of memory. For all runs with more than 15 cores, on each node we ran 15 compute jobs and one job for interfacing with the storage system. Since the storage jobs use negligible computation time, we omit them from the CPU core count when determining speedup and efficiency.

nodes	cores	runtime	speedup	efficiency
1	1	122857.6	1.000	1.000
1	15	9837.8	12.488	0.832
2	30	4954.8	24.795	0.826
4	60	2625.4	46.794	0.779
8	120	1341.3	91.592	0.763
14	210	952.3	129.011	0.614
15	225	705.6	174.113	0.773
16	240	694.3	176.929	0.737
29	435	611.8	200.810	0.461
30	450	385.4	318.747	0.708
32	480	379.9	323.310	0.673
40	600	367.7	334.109	0.556
48	720	363.2	338.178	0.469

Table 1. Timings and efficiency for cut $\{1, 3, 4, 5\}$. We use the same algorithm for all core counts. The single core run serves as a reference.

Apart from the running time $T(n)$ of the algorithm on a total of n cores, we also give the speedup $S(n) = \frac{T(1)}{T(n)}$ and the efficiency $E(n) = \frac{T(1)}{nT(n)}$, which measure how “well” the algorithm parallelizes with increasing core counts. Note that the single-core timing is somewhat special: As experiments have shown the performance per core decreases with the number of cores used on a given node. This effect has been investigated in [67] (see in particular [67, Figure 5]). Thus, for the analysis of the expected run-time below, we rather use the baseline of 83.2% efficiency on 15 cores.

The saw-tooth shape of the efficiency graph in Figure 6 (and the corresponding behavior in the timing and speedup graphs) is due to the fact that the number of reductions to execute is usually not divisible by the number of cores utilized. Since in our test problem approximately 450 reductions are required to enable the final interpolation, the running time of the full algorithm is roughly

$$\left\lceil \frac{450}{\text{number of CPUs}} \right\rceil. \quad (4.2)$$

This effect can be avoided by a more fine-grained structuring of the problem (for instance by interpolating more parameters).

Additionally, Figure 6 depicts the ideal expected runtime, speedup and efficiency. These ideal graphs stem from the simple assumption, called *Amdahl’s law*, that an algorithm can

³Hypertexting is disabled.

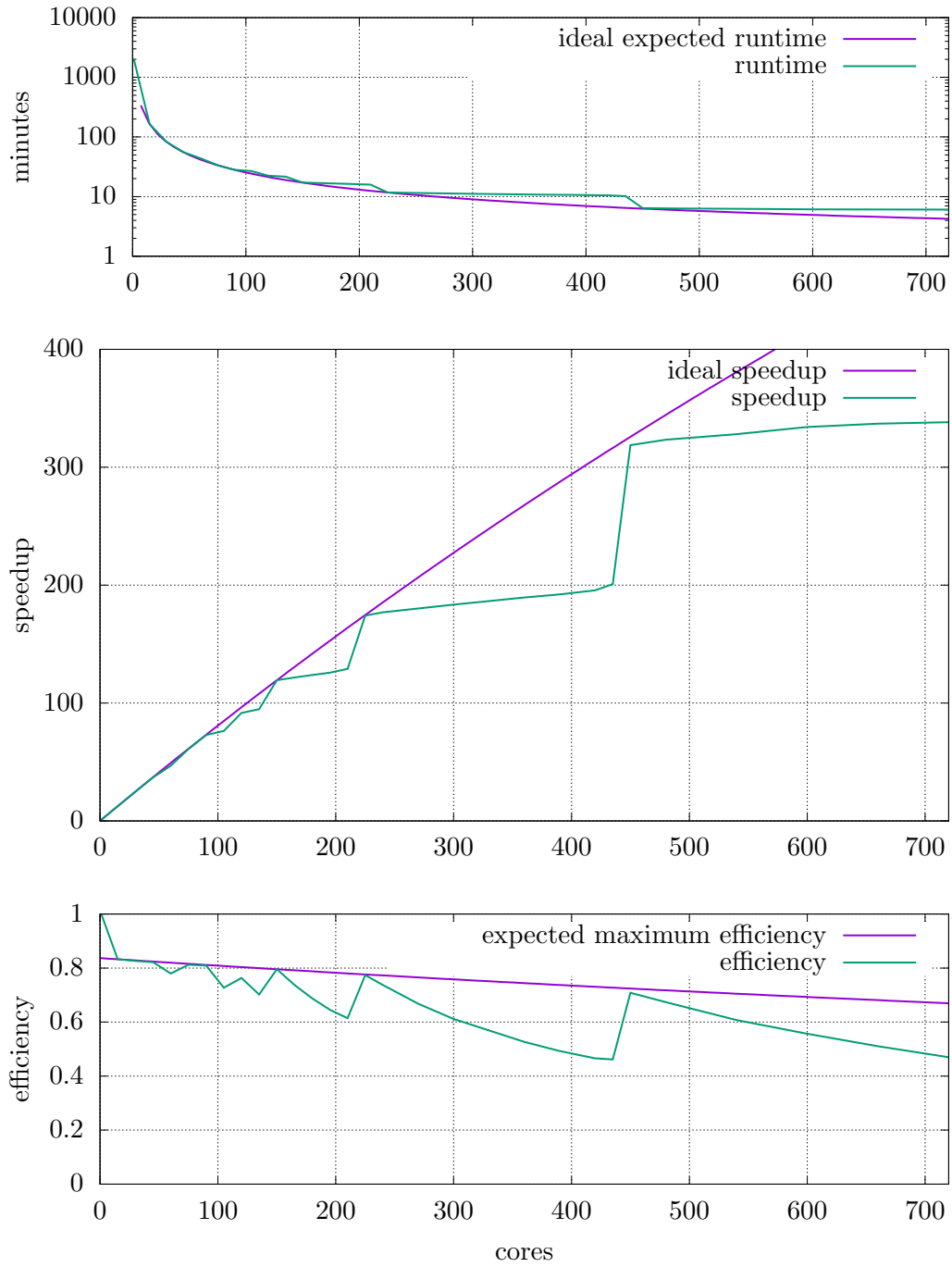


Figure 6. Running time and efficiency graphs for cut $\{1, 3, 4, 5\}$

be partitioned into a part that is ideally parallelizable and a part which is not parallelizable at all. Denoting the parallelizable fraction by f , the expected runtime $T_{\text{ideal}}(n)$ on n cores is not $\frac{T(1)}{n}$, but rather

$$T_{\text{ideal}}(n) = (1 - f) \cdot T(1) + \frac{f \cdot T(1)}{n} \quad (4.3)$$

which yields ideal speedup and efficiency

$$S_{\text{ideal}}(n) = \frac{n}{(1-f) \cdot n + f}, \quad E_{\text{ideal}}(n) = \frac{1}{(1-f) \cdot n + f}. \quad (4.4)$$

Using the experimental values for 15 and 30 cores, we arrive at a value $f \approx 0.9948$, that is, only 0.52 % of the algorithm is not parallelizable.

As we can see, the ideal curves give a fairly tight bound on the actual timings, at least in the cases where the core count is properly aligned to the number of reductions. This indicates that our approach for parallelization not only provides an automatic and fast solution to a tedious and complicated task, but stays highly efficient even when used with a large amount of computing power.

5 IBP conversion between different integral bases

It is well known that the IBP coefficient size can be quite different by choosing different master integral bases. In this section, we observe that for a complicated multi-loop diagram, the IBP coefficients are significantly smaller in the uniformly transcendental (UT) basis [18].

We prefer the IBP reduction to a UT basis for several reasons: a) A UT integral basis has a very simple form of differential equations [18] which allows for the integrals to be solved analytically in terms of polylogarithms. There is also evidence that for numerical computations, the UT basis is more convenient to evaluate⁴. So the IBP reduction to a UT basis greatly simplifies the amplitude computations after the IBP reduction. b) We find examples for which the IBP coefficients in a UT basis are significantly simpler than these in a traditional Laporta basis. This makes the IBP coefficients easier to use. Furthermore, in this case, if only the IBP coefficients in a UT basis are needed, we can carry out a “semi-numerical” approach to get the UT basis IBP coefficients with fewer numeric points.

In practice, we apply a special form of UT basis, the so-called dlog basis, which is introduced in the next subsection.

5.1 Dlog basis definition and the dlog algorithm

We call a Feynman integral a dlog integral if its integrand can be written as a sum of dlog forms [72]. Given a differential n -form depending on n -variables

$$dI = dx_1 \wedge dx_2 \wedge \dots \wedge dx_n R(x_1, \dots, x_n), \quad (5.1)$$

where $R(x_1, \dots, x_n)$ is a rational function in x_1, \dots, x_n , we say dI has a dlog form if it can be written as

$$dI = \sum_i c_i d\log f_{i,1} \wedge \dots \wedge d\log f_{i,n}, \quad (5.2)$$

with $f_{i,j}$ being algebraic functions of x_1, \dots, x_n .

Writing an integrand form as a sum of dlog forms makes the property manifest that it has only simple poles. Thus, whenever an integrand has a pole of higher degree than one, we know that it has no dlog forms. This also applies for points at infinity. So both $\frac{dx}{x^2}$ and dx have no dlog forms because of double poles at zero or at infinity.

The coefficients c_i in equation (5.2) are called leading singularities [73]. For Feynman integrals they are in general algebraic functions of the external variables. The leading singularities can also be understood as integrals over the original integrand where the integration contour is localized around the poles of the integrand. Leading singularities and the integrals integrated on the real contour have analytic properties in common. So, integrals with leading singularities that are just constant numbers are particularly useful, most importantly because they fulfill differential equations in the canonical form [18]. This implies that they have the property of uniform transcendental weight, which means that if series expanded in ϵ , the parameter of dimensional regularization, the coefficients have homogeneous transcendental weight and the weight increases by one for each order in ϵ .

⁴Private communication with Yang Gang.

Next, we discuss how to write a given integrand as a sum of dlog forms using the approach of [62]. Given an integrand in n integration variables we choose one variable x that is linear in all denominator factors and do a partial fraction decomposition while treating all other variables as constants. This way we obtain a sum of integrands of the form

$$\frac{dx}{x-a} \wedge \Omega = d \log(x-a) \wedge \Omega, \quad (5.3)$$

where Ω is an $(n-1)$ -form, independent of x , and a is a polynomial that may depend on the other integration variables. Then we iterate this procedure taking Ω as our new integrand until no integration variables are left. If in any intermediate step a pole of degree two or higher is encountered then the integrand does not have a dlog form. There are cases where no variable exists that is linear in all denominator factors. One way to proceed in such a case is to make a variable transformation such that at least one of the new variables is linear in all denominator factors.

The algorithmic approach of this section was used in [74] and [75] to construct a complete basis of dlog master integrals with constant leading singularities for all two-loop five point integral families. The denominator structure for each integral family is given by the propagators. To construct the dlog integrals we make a general numerator ansatz. We write the numerator as a linear combination of terms that are products of inverse propagators and irreducible scalar products. Each term is multiplied by a free parameter and by applying the algorithm on this general integrand we can determine values of the free parameters such that the integrand has a dlog form and constant leading singularities. The solutions we find for the free parameters are in general algebraic functions of the external variables. Inserting the solutions for the free parameters in the initial numerator ansatz we obtain a set of dlog integrals that form a basis of dlog master integrals.

In general the dlog algorithm can be applied only in a dimension that is an integer number, which we choose to be four. The loop momenta are very conveniently parametrized using spinor helicity variables as in [72]. This parametrization being very useful has also its limitations as soon as the numerator has terms that vanish in strictly four dimensions but which are non-zero in D -dimensions. In such cases an extended approach can be used as in [75] using Baikov parametrization.

5.2 IBP reduction with a dlog basis

With a dlog basis, we consider the IBP reduction computation in two cases:

1. When both the IBP coefficients in a Laporta basis and the dlog basis are needed, we first compute the reduction in the Laporta basis I with our module intersection and GPI-SPACE reduction algorithm.

$$F = AI \quad (5.4)$$

where F is the list of target integrals as a column vector. Then we reduce the dlog basis \tilde{I} to the Laporta basis I ,

$$\tilde{I} = TI \quad (5.5)$$

Note that since the dlog basis construction has a restriction of the numerator degree, this reduction is usually easy. Then using our SINGULAR RREF code, with a good pivot strategy, we can analytically find the inverse T^{-1} . The matrix product AT^{-1} contains the coefficients of IBP reduction to the dlog basis.

We remark that the product AT^{-1} can be difficult to calculate even if T^{-1} has a relative small size. Instead of computing the production directly, we again use the “semi-numerical” approach, to set several of the kinematics values as integers, compute the product several times, and then use our interpolation program to get the fully analytical matrix production AT^{-1} . This is again implemented with our GPI-SPACE computer algebra.

2. When only the IBP coefficients in a dlog basis are needed, we use our “semi-numerical” reduction method to a set of numeric IBP coefficients in the Laporta basis. Instead of interpolating these coefficients, we compute the product AT^{-1} for these semi-numeric points. And then we interpolate to get AT^{-1} analytically and the analytic form of A is not calculated.

We demonstrate our module intersection IBP, GPI space massive parallelization for reduction, and basis conversion by a non-trivial example, the two-loop five-point nonplanar double pentagon diagram in the next section.

6 Two-loop five-point nonplanar double pentagon example

We demonstrate the capabilities of our efficient IBP method using SINGULAR and GPI-SPACE by executing the analytic IBP reduction for a nontrivial example, the two-loop five-point nonplanar double pentagon integral. The symbolic representation of the UT integral basis of this integral family was found in [5, 11]. Furthermore, the UT integral basis of this integral family, as well as all other two-loop five-point nonplanar massless integral families were analytically calculated in terms of polylogarithm functions in [75].

For the diagram in Figure 7, we chose the following labeling for the propagators:

$$\begin{aligned}
D_1 &= l_1^2 & D_2 &= (l_1 - k_1)^2 & D_3 &= (l_1 - k_{12})^2 & D_4 &= l_2^2 \\
D_5 &= (l_2 - k_{123})^2 & D_6 &= (l_2 - k_{1234})^2 & D_7 &= (l_1 - l_2)^2 & D_8 &= (l_1 - l_2 + k_3)^2 \\
D_9 &= (l_1 - k_{1234})^2 & D_{10} &= (l_2 - k_1)^2 & D_{11} &= (l_2 - k_{12})^2, & &
\end{aligned} \tag{6.1}$$

where l_i 's represent the loop momenta, k_i 's represent external momenta and $k_{i\dots j} = \sum_i^j k_i$, the first 8 propagators represent the topology and the last three the irreducible scalar products.

This is a complicated integral family for IBP reduction, due to 6 scalars, which are s12, s23, s34, s45, s45, s15 and the spacetime dimension D, and due to the nonplanar topology with two pentagons inside. We demonstrate our method by reducing the following 26

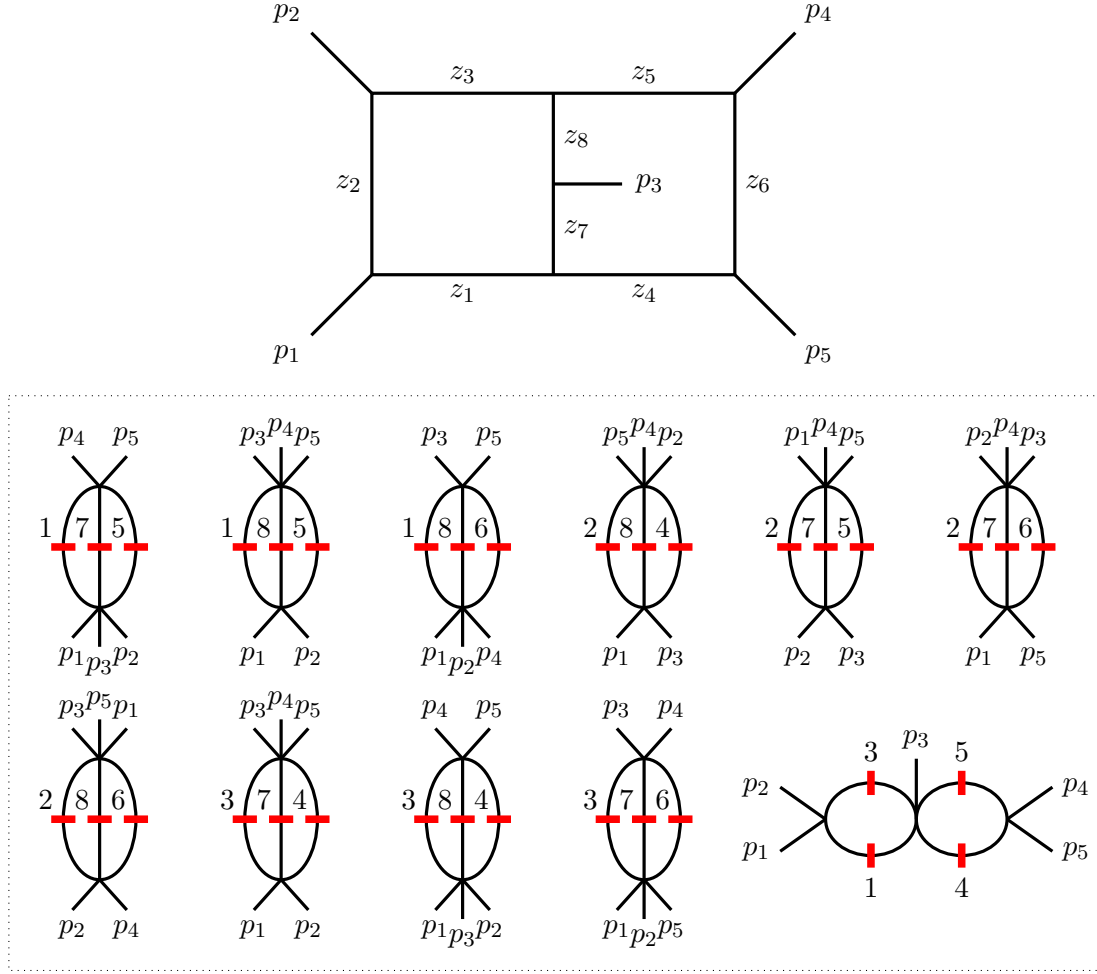


Figure 7. Two-loop five-point nonplanar double pentagon diagram. The z_i are the Baikov variables, equal to the inverse propagators. In particular, $z_1 = l_1^2$ and $z_4 = l_2^2$. We also draw the 11 spanning cuts of this integral family, and the corresponding non-collapsible master integrals, before using symmetries.

integrals up to a numerator degree of 4,

$$\begin{aligned}
& I[1, 1, 1, 1, 1, 1, 1, 1, 0, 0, -4], I[1, 1, 1, 1, 1, 1, 1, 1, 0, -1, -3], I[1, 1, 1, 1, 1, 1, 1, 1, 0, -2, -2], \\
& I[1, 1, 1, 1, 1, 1, 1, 1, 0, -3, -1], I[1, 1, 1, 1, 1, 1, 1, 1, 0, -4, 0], I[1, 1, 1, 1, 1, 1, 1, 1, -1, 0, -3], \\
& I[1, 1, 1, 1, 1, 1, 1, 1, -1, -1, -2], I[1, 1, 1, 1, 1, 1, 1, 1, -1, -2, -1], I[1, 1, 1, 1, 1, 1, 1, 1, -1, -3, 0], \\
& I[1, 1, 1, 1, 1, 1, 1, 1, -2, 0, -2], I[1, 1, 1, 1, 1, 1, 1, 1, -2, -1, -1], I[1, 1, 1, 1, 1, 1, 1, 1, -2, -2, 0], \\
& I[1, 1, 1, 1, 1, 1, 1, 1, -3, 0, -1], I[1, 1, 1, 1, 1, 1, 1, 1, -3, -1, 0], I[1, 1, 1, 1, 1, 1, 1, 1, -4, 0, 0], \\
& I[1, 1, 1, 1, 1, 1, 1, 1, 0, 0, -3], I[1, 1, 1, 1, 1, 1, 1, 1, 0, -1, -2], I[1, 1, 1, 1, 1, 1, 1, 1, 0, -2, -1], \\
& I[1, 1, 1, 1, 1, 1, 1, 1, 0, -3, 0], I[1, 1, 1, 1, 1, 1, 1, 1, -1, 0, -2], I[1, 1, 1, 1, 1, 1, 1, 1, -1, -1, -1], \\
& I[1, 1, 1, 1, 1, 1, 1, 1, -1, -2, 0], I[1, 1, 1, 1, 1, 1, 1, 1, -2, 0, -1], I[1, 1, 1, 1, 1, 1, 1, 1, -2, -1, 0], \\
& I[1, 1, 1, 1, 1, 1, 1, 1, -3, 0, 0], I[1, 1, 1, 1, 1, 1, 1, 1, 0, 0, -2] \tag{6.2}
\end{aligned}$$

to the master integral basis in the fashion of Laporta. Furthermore, we convert the IBP coefficients to the coefficients of a dlog basis given in [75]. In this base change, we observe a significant coefficient size reduction.

6.1 Module intersection with cuts

First, we use AZURITE [46] to find an integral basis. Without considering symmetries, there are 113 irreducible integrals, and with symmetries, there are 108 master integrals. Note that due to the number of master integrals, this IBP reduction is significantly more complicated than the reduction of the hexagon-box diagram in [58], which has only 73 master integrals.

We can then construct the set of spanning cuts of this integral family. Each spanning cut corresponds to a “non-collapsible” master integral [46]. There are 11 spanning cuts (without considering symmetries)

$$\begin{aligned} & \{1, 5, 7\}, \{1, 5, 8\}, \{1, 6, 8\}, \{2, 4, 8\}, \{2, 5, 7\}, \{2, 6, 7\}, \\ & \{2, 6, 8\}, \{3, 4, 7\}, \{3, 4, 8\}, \{3, 6, 7\}, \{1, 3, 4, 5\} \end{aligned} \quad (6.3)$$

where the numbers indicate the propagators on cut. For example, $\{3, 4, 7\}$ means that $D_3 \mapsto 0, D_4 \mapsto 0, D_7 \mapsto 0$.

For each cut, we can apply our module intersection method to generate IBPs without doubled propagators. In [58], the IBPs are generated only from the top sector. Here, for each cut, we generate the IBPs from both the top sector and lower sectors. For example, for the cut $\{1, 5, 7\}$, we consider the 32 sectors supported on cut $\{1, 5, 7\}$, and compute all the module intersections. This approach will generate more IBPs but make the IBP system more block-triangular and easier for linear reduction.

With the **degbound** option in SINGULAR, it is easy to generate all the module intersections. For this integral family, with the degree bound 5, we find that, with one core for each cut, it takes less than 5 minutes in total to solve all the module intersection problems *analytically*. Later on, by finite-field methods, we find that this degree bound generates sufficient IBPs for our problem.

After generating the IBPs, we use the two-step trimming process described in Section 2.2, to select necessary IBPs for our targets. This computation is via finite-field methods and powered by the package SPASM.

Note that different cuts can support the same master integral, we call this cut overlap. For example, cuts $\{1, 5, 7\}$ and $\{2, 4, 8\}$ both supports the integral $I[1, 1, 1, 1, 1, 0, 1, 1, 0, 0, 0]$. The IBP reductions on these two cuts should give the same coefficients. To avoid redundant computations, we can apply the master integral removal method [48], to set $I[1, 1, 1, 1, 1, 0, 1, 1, 0, 0, 0] \mapsto 0$ in either cut $\{1, 5, 7\}$ or $\{2, 4, 8\}$. Clearly there are many different removal strategies for master integral overlapping in different cuts, and different strategies result in different performances. In this computation, heuristically, we find that the cuts $\{1, 6, 8\}$ and $\{2, 4, 8\}$ are relatively “difficult” cuts for IBP reduction. Hence, we set as many master integrals as possible in $\{1, 6, 8\}$ and $\{2, 4, 8\}$ to zero, and later on recover the remaining master integral coefficients from other cuts via cut overlap.

We compute the module intersection analytically. For the purpose of linear reduction, we further set

$$s_{12} \mapsto 1, \quad c_2 \equiv s_{23}/s_{12}, \quad c_3 \equiv s_{34}/s_{12}, \quad c_4 \equiv s_{45}/s_{12}, \quad c_5 \equiv s_{15}/s_{12}, \quad (6.4)$$

to dehomogenize the IBP relations and speed up the computation. The s_{12} dependence can be recovered in the final step.

The resulting IBPs are summarized in Table 2. Note that for cut $\{1, 6, 8\}$ there are 1203 independent relations and 1205 integrals, since we apply the idea [48] to set most master integrals supported on cut $\{1, 6, 8\}$ as zero and we just compute two master integral coefficients.

Cut	# relations	# integrals	size	d_2	d_3
$\{1, 5, 7\}$	1134	1182	0.77 MB	21	22
$\{1, 5, 8\}$	1141	1192	0.85 MB	18	18
$\{1, 6, 8\}$	1203	1205	1.1 MB	19	30
$\{2, 4, 8\}$	1245	1247	1.1 MB	35	24
$\{2, 5, 7\}$	1164	1211	0.84 MB	26	18
$\{2, 6, 7\}$	1147	1206	0.62 MB	16	17
$\{2, 6, 8\}$	1126	1177	0.83 MB	16	18
$\{3, 4, 7\}$	1172	1221	0.78 MB	19	18
$\{3, 4, 8\}$	1180	1226	1.0 MB	19	22
$\{3, 6, 7\}$	1115	1165	0.82 MB	21	28
$\{1, 3, 4, 5\}$	721	762	0.43MB	14	14

Table 2. IBP relations generated on each cut by the module intersection method. We used finite-field methods to pick linear independent and necessary IBP relations. The size is the output file size on disk before reduction. The numbers d_2 and d_3 are the maximal degrees in the reduced IBP relations for c_2 and c_3 , respectively.

6.2 IBP reduction

We use our reduction method via SINGULAR and GPI-SPACE to reduce the linear systems in Table 2. We apply a semi-numeric approach, setting c_4 , c_5 and the space-time dimension D symbolic, and compute the linear reduction with integer-valued c_2 and c_3 .

By a linear reduction with c_2 (c_3) symbolic and all the other parameters numeric, we easily determine the maximal degree of c_2 (c_3) in the reduced IBP relations. The degrees are listed in Table 2. From this information, we get the minimal number $(d_2+1) \times (d_3+1)$ of semi-numeric computations for interpolating the analytic reduction result. For example, for the cut $\{1, 5, 7\}$, we need to run semi-numeric computations at least 506 times. Of course, the cuts exhibit different running times when performing the reductions: For instance, cut $\{1, 3, 4, 5\}$, which we already considered as an example in Section 4.4, is the easiest in terms of running time, taking only about 11 minutes when using 384 CPU cores. In contrast, the cut $\{3, 4, 6\}$ is much more complex: its reduction took 12 hours and 21 minutes, using 384 cores.

After getting the analytic reduction of all the cuts, we merge them to get the full IBP reduction to a 113 integral basis. Furthermore, we apply the symmetries, obtained from [46],

$$I[0, 0, 1, 1, 0, 0, 0, 1, 0, 0, 0] = I[1, 0, 0, 0, 1, 0, 1, 0, 0, 0, 0] \quad (6.5)$$

$$I[0, 0, 1, 1, 0, 0, 1, 0, 0, 0, 0] = I[1, 0, 0, 0, 1, 0, 0, 1, 0, 0, 0] \quad (6.6)$$

$$I[1, 0, 1, 0, 1, 0, 1, 0, 0, 0, 0] = I[1, 0, 1, 1, 0, 0, 0, 1, 0, 0, 0] \quad (6.7)$$

$$I[0, 0, 1, 1, 1, 0, 1, 0, 0, 0, 0] = I[1, 0, 0, 1, 1, 0, 0, 1, 0, 0, 0] \quad (6.8)$$

$$I[1, 0, 1, 1, 1, 0, 0, 1, 0, 0, 0] = I[1, 0, 1, 1, 1, 0, 1, 0, 0, 0, 0] \quad (6.9)$$

to reduce the 26 target integrals to a 108-integral Laporta basis I . We note that the resulting file is large, with a size of ~ 2.0 GB on disk.

By setting all Mandelstam variables as integers, we have verified that our result is consistent with FIRE6 [37].

6.3 IBP coefficients conversion to dlog basis

In this subsection, we discuss converting the IBP coefficients for the Laporta basis to the IBP coefficients of a dlog basis in [75].

Again we use the semi-numeric approach for this IBP coefficients conversion: taking integer-valued c_2 , c_3 and symbolic c_4 and c_5 , D , convert the coefficients and then interpolate. It is easy to determine that the coefficients in the dlog basis, have the following maximal degrees for c_2 and c_3 respectively,

$$d'_2 = 20, \quad d'_3 = 20 \quad (6.10)$$

Then we directly see by comparing with Table 2, where d_2 can be as high as 35, that the maximal degree drops. For the basis conversion, we carry out a semi-numeric matrix multiplication with subsequent interpolation using SINGULAR and GPI-SPACE.

After the computation, we see that the IBP reduction coefficients of (6.2) in this dlog basis have a size of 480 MB on disk. In this case, this is a significant 76% reduction of the IBP coefficient size, comparing with those for the Laporta basis. On the other hand, if we only need the IBP reduction coefficients in the dlog basis, we can skip the interpolation for the Laport basis IBP coefficients and directly convert the numeric intermediate results to dlog basis IBP coefficients. Because of the maximal degree drop, this shortcut reduces the number of semi-numeric computations required.

For convenience, we also provide the IBP coefficients in the dlog basis, with the s_{12} scalar recovered. All these analytic results are uploaded to the links presented in the introduction of this paper. Note that all files from the links, are 26×108 matrices. The i -th row and j -th column is the corresponding IBP coefficient for the i -th target integral in 6.2 expanded on the j -th master integral. The Laporta basis and the dlog basis are included in the auxiliary files of this paper.

7 Summary

In this paper, we present our powerful new IBP reduction methods, based on computational algebraic geometry powered by the computer algebra system SINGULAR in conjunction with the taskflow management system GPI-SPACE. Our method is suitable for large scale IBP reduction problems with complicated Feynman diagrams and multiple variables. We demonstrate the power of our new method by the analytic two-loop five-point nonplanar double pentagon IBP computation. The computational result has been cross-checked numerically using the state-of-the-art IBP programs.

Our method is flexible and can be adapted in various different scenarios:

1. Modern amplitudes computations often prefer to compute IBP numerically or semi-numerically many times, and interpolate the amplitude coefficient directly instead of interpolating the analytic IBP coefficients. Our method can efficiently compute the reduced numeric or semi-numeric IBP relations, and hence perfectly fits into this purpose.
2. Our module intersection method, can also be used for integrals with doubled propagators or multiple-power propagators, since this IBP generating method avoids the increase of propagator exponents and significantly reduces the size of the IBP system.
3. Although currently our method is based on semi-numerical parallelizations with integer-valued numerics, clearly this method can be extended to finite-field linear reduction, if necessary.
4. More generally, our linear reduction parallelization method can be used for computational problems other than IBP reduction. For example, in recent years, it was found that the Bethe Ansatz equation of integrable spin chains can be analytically computed by algebraic geometry methods [76, 77]. Often this computation involves large-scale linear algebra computations with symbolic parameters, and our parallelization via the SINGULAR-GPI-SPACE framework can greatly speed up the computation. We also expect that our reduction method can be used more generally for Gröbner basis computations with parameters.

In the future, we will develop our code into an automated software package, powered by SINGULAR and GPI-SPACE, for solving large-scale IBP or amplitude problems. The possible simplification of IBP coefficients in a UT/dlog basis will be further investigated. We expect that this method will provide a boost for the current NNLO precision computations.

Acknowledgments

YZ thank Johann Usövitsch for many enlightening discussions on IBP reduction algorithms and their implementation, and Johannes Henn for cutting-edge techniques for finding uniformly transcendental and dlog integrals. We acknowledge Kasper Larsen for his work in the starting stage of the analysis of the two-loop nonplanar five-point double pentagon

diagram. We thank Simon Badger, Rutger Boels, Christian Bogner, Hjalte Frellesvig, Gudrun Heinrich, Harald Ita, Stephan Jahn, David Kosower, Roman Lee, Hui Luo, Yanqing Ma, Andreas von Manteuffel, Pierpaolo Mastrolia, Erik Panzer, Tiziano Peraro, Robert Schabinger, Hans Schönemann, Alexander Smirnov, Vladimir Smirnov, Peter Uwer, Gang Yang and Mao Zeng for their help on this research project.

The research leading to these results has received funding from Swiss National Science Foundation (Ambizione grant PZ00P2 161341), from the National Science Foundation under Grant No. NSF PHY17-48958, from the NSF of China with Grant No. 11235010, from the European Research Council (ERC) under the European Unions Horizon 2020 research and innovation programme (grant agreement No 725110). The work of AG is supported by the Knut and Alice Wallenberg Foundation under grant #2015-0083. The work of DB and JB was supported by Project IL5 of SFB-TRR 195 *Symbolic Tools in Mathematics and their Application* of the German Research Foundation (DFG). The authors would also like to express a special thanks to the Mainz Institute for Theoretical Physics (MITP) of the Cluster of Excellence PRISMA+ (Project ID 39083149) for its hospitality and support, during the “Mathematics of Linear Relations between Feynman Integrals” workshop.

A Rational function interpolation

In this appendix, we introduce our simple approach to rational function interpolation. Although this algorithm is rather straight-forward compared to other more involved techniques available, e.g. in [78–80], we have found that it is more suitable for our setup. The idea is to heuristically convert a rational function interpolation problem to a polynomial function interpolation problem.

We focus on a general computation process with symbolic variables x_1, \dots, x_k which would give the final result as a rational function

$$\frac{F(x_1, \dots, x_k)}{G(x_1, \dots, x_k)}. \quad (\text{A.1})$$

Here F and G are integer valued polynomials with $\gcd(F, G) = 1$. Suppose that this computation is difficult with symbolic parameters x_1, \dots, x_k , but doable when only part of the parameters are symbolic and the rest of the parameters are set to general integer values. Our goal is to repeat this semi-numeric computation N times, and interpolate to get (A.1).

To be specific, we call the computation with symbolic x_{k_1+1}, \dots, x_k ($k_1 < k$) and the evaluation

$$x_1 \mapsto a_1^{(i)}, \quad \dots, \quad x_{k_1+1} \mapsto a_{k_1+1}^{(i)} \quad (\text{A.2})$$

the i -th semi-numeric computation. Here $a_j^{(i)}$'s are usually chosen as random integers. The i -th semi-numeric computation gives the result,

$$\frac{f_i(x_{k_1+1}, \dots, x_k)}{g_i(x_{k_1+1}, \dots, x_k)}. \quad (\text{A.3})$$

Note that, although computer algebra software can cancel the fraction to get polynomials f_i and g_i with $\gcd(f_i, g_i) = 1$, the relation between G and g is not clear. Sometimes,

$$g_i(x_{k_1+1}, \dots, x_k) \neq G(a_1^{(i)}, \dots, a_k^{(i)}, x_{k_1+1}, \dots, x_k) \quad (\text{A.4})$$

and also,

$$f_i(x_{k_1+1}, \dots, x_k) \neq F(a_1^{(i)}, \dots, a_k^{(i)}, x_{k_1+1}, \dots, x_k) \quad (\text{A.5})$$

The reason is that after taking integer values $a_1^{(i)}, \dots, a_k^{(i)}$ for the first k variables, there can be additional cancellations between F and G . This phenomenon makes the direct polynomial interpolation of the g_i and f_i inapplicable.

We solve this cancellation problem in a heuristic way.

1. First, we compute a “reference” result with symbolic x_1, \dots, x_k and generic integer values for $x_{k_1+1} \dots x_k$, ($x_{k_1+1} \mapsto b_{k_1}, \dots, x_k \mapsto b_k$).

$$\frac{p(x_1, \dots, x_{k_1})}{q(x_1, \dots, x_{k_1})}. \quad (\text{A.6})$$

where p and q are integer valued polynomials and $\gcd(p, q) = 1$. Generally, except for a statistically very small set of values of b , we can assume that the two polynomials $F(x_1, \dots, x_{k_1}, b_{k_1+1}, \dots, b_k)$ and $G(x_1, \dots, x_{k_1}, b_{k_1+1}, \dots, b_k)$ have the greatest common factor in \mathbb{Z} . Then since,

$$\frac{p(x_1, \dots, x_{k_1})}{q(x_1, \dots, x_{k_1})} = \frac{F(x_1, \dots, x_{k_1}, b_{k_1+1}, \dots, b_k)}{G(x_1, \dots, x_{k_1}, b_{k_1+1}, \dots, b_k)} \quad (\text{A.7})$$

by the unique factorization domain (UFD) property,

$$G(x_1, \dots, x_{k_1}, b_{k_1+1}, \dots, b_k) = \mu \cdot q(x_1, \dots, x_{k_1}) \quad (\text{A.8})$$

$$F(x_1, \dots, x_{k_1}, b_{k_1+1}, \dots, b_k) = \mu \cdot p(x_1, \dots, x_{k_1}) \quad (\text{A.9})$$

where μ is an integer. The value of μ is not determined yet in this step, and actually only the existence of μ is needed for our algorithm.

2. Second, we do a “majority vote” selection of the semi-numeric results. Of each of the semi-numeric results, we record the leading monomial’s exponent in x_{k_1+1}, \dots, x_k . The most common exponent is denoted as \mathbf{r} . We drop semi-numeric result whose exponent is not equal to \mathbf{r} . This step ensures that the gcd of $F(a_1^{(i)}, \dots, a_k^{(i)}, c_{k_1+1}, \dots, c_k)$ and $G(a_1^{(i)}, \dots, a_k^{(i)}, x_{k_1+1}, \dots, x_k)$ is just an integer instead of a non-constant polynomial in x_{k_1+1}, \dots, x_k . Again by the UFD property,

$$G(a_1^{(i)}, \dots, a_k^{(i)}, x_{k_1+1}, \dots, x_k) = \lambda_i \cdot g_i(x_{k_1+1}, \dots, x_k) \quad (\text{A.10})$$

$$F(a_1^{(i)}, \dots, a_k^{(i)}, x_{k_1+1}, \dots, x_k) = \lambda_i \cdot f_i(x_{k_1+1}, \dots, x_k) \quad (\text{A.11})$$

where λ_i is an integer. Set $x_1 \mapsto a_1^{(i)}, \dots, x_{k_1+1} \mapsto a_{k_1+1}^{(i)}$ in (A.8) and $x_{k_1+1} \mapsto b_{k_1}, \dots, x_k \mapsto b_k$ in (A.10), we determine that

$$\lambda_i = \mu \frac{q(a_1^{(i)}, \dots, a_{k_1}^{(i)})}{g_i(b_{k_1+1}, \dots, b_k)} \quad (\text{A.12})$$

3. Define

$$\tilde{g}_i(x_{k_1+1}, \dots, x_k) \equiv \frac{\lambda_i}{\mu} g_i(x_{k_1+1}, \dots, x_k) = \frac{q(a_1^{(i)}, \dots, a_{k_1}^{(i)})}{g_i(b_{k_1+1}, \dots, b_k)} g_i(x_{k_1+1}, \dots, x_k) \quad (\text{A.13})$$

$$\tilde{f}_i(x_{k_1+1}, \dots, x_k) \equiv \frac{\lambda_i}{\mu} f_i(x_{k_1+1}, \dots, x_k) = \frac{q(a_1^{(i)}, \dots, a_{k_1}^{(i)})}{g_i(b_{k_1+1}, \dots, b_k)} f_i(x_{k_1+1}, \dots, x_k) \quad (\text{A.14})$$

and then interpolate both polynomials $\tilde{f}_i(x_{k_1+1}, \dots, x_k)$ and $\tilde{g}_i(x_{k_1+1}, \dots, x_k)$ for the selected semi-numeric points by usual polynomial interpolation algorithms, say using Newton polynomials. From (A.12), we see that the resulting two polynomials are,

$$\frac{1}{\mu} F(x_1, \dots, x_k, x_{k_1+1}, \dots, x_k), \quad \frac{1}{\mu} G(x_1, \dots, x_k, x_{k_1+1}, \dots, x_k). \quad (\text{A.15})$$

The ratio of the two polynomials gives the computation goal F/G while the integer factor μ canceled out.

So with the compensation factors λ_i/μ , we used the simple polynomial interpolation to interpolate rational functions, at the extra cost of computing only one additional reference point. If the maximal power of x_j ($1 \leq j \leq k_1$) in F and G is d_j , generically, we need to compute the semi-numeric result

$$(d_1 + 1) \times \dots \times (d_{k_1} + 1) \quad (\text{A.16})$$

times, plus one computation for the reference point.

The algorithm is implemented in the computer algebra system SINGULAR and GPI-SPACE.

In practice, this algorithm is extendable in many ways: for example, instead of splitting the variables x_1, \dots, x_k into two groups (x_1, \dots, x_{k_1}) and (x_{k_1+1}, \dots, x_k) , we can split the variables in more groups and use our algorithm recursively. The algorithm can also be combined with finite field reconstruction.

References

- [1] S. Badger, H. Frellesvig, and Y. Zhang, *A Two-Loop Five-Gluon Helicity Amplitude in QCD*, *JHEP* **12** (2013) 045, [[arXiv:1310.1051](#)].
- [2] T. Gehrmann, J. M. Henn, and N. A. Lo Presti, *Analytic form of the two-loop planar five-gluon all-plus-helicity amplitude in QCD*, *Phys. Rev. Lett.* **116** (2016), no. 6 062001, [[arXiv:1511.05409](#)]. [Erratum: *Phys. Rev. Lett.* 116, no. 18, 189903 (2016)].
- [3] S. Badger, C. Brnnum-Hansen, H. B. Hartanto, and T. Peraro, *First look at two-loop five-gluon scattering in QCD*, *Phys. Rev. Lett.* **120** (2018), no. 9 092001, [[arXiv:1712.02229](#)].
- [4] S. Abreu, F. Febres Cordero, H. Ita, B. Page, and M. Zeng, *Planar Two-Loop Five-Gluon Amplitudes from Numerical Unitarity*, *Phys. Rev.* **D97** (2018), no. 11 116014, [[arXiv:1712.03946](#)].
- [5] S. Abreu, L. J. Dixon, E. Herrmann, B. Page, and M. Zeng, *The two-loop five-point amplitude in $\mathcal{N} = 4$ super-Yang-Mills theory*, *Phys. Rev. Lett.* **122** (2019), no. 12 121603, [[arXiv:1812.08941](#)].

- [6] S. Abreu, F. Febres Cordero, H. Ita, B. Page, and V. Sotnikov, *Planar Two-Loop Five-Parton Amplitudes from Numerical Unitarity*, *JHEP* **11** (2018) 116, [[arXiv:1809.09067](#)].
- [7] R. H. Boels, Q. Jin, and H. Luo, *Efficient integrand reduction for particles with spin*, [arXiv:1802.06761](#).
- [8] T. Gehrmann, J. M. Henn, and N. A. Lo Presti, *Pentagon functions for massless planar scattering amplitudes*, *JHEP* **10** (2018) 103, [[arXiv:1807.09812](#)].
- [9] S. Badger, C. Brnnum-Hansen, H. B. Hartanto, and T. Peraro, *Analytic helicity amplitudes for two-loop five-gluon scattering: the single-minus case*, *JHEP* **01** (2019) 186, [[arXiv:1811.11699](#)].
- [10] S. Abreu, J. Dormans, F. Febres Cordero, H. Ita, and B. Page, *Analytic Form of Planar Two-Loop Five-Gluon Scattering Amplitudes in QCD*, *Phys. Rev. Lett.* **122** (2019), no. 8 082002, [[arXiv:1812.04586](#)].
- [11] D. Chicherin, T. Gehrmann, J. M. Henn, P. Wasser, Y. Zhang, and S. Zoia, *Analytic result for a two-loop five-particle amplitude*, *Phys. Rev. Lett.* **122** (2019), no. 12 121602, [[arXiv:1812.11057](#)].
- [12] D. Chicherin, T. Gehrmann, J. M. Henn, P. Wasser, Y. Zhang, and S. Zoia, *The two-loop five-particle amplitude in $\mathcal{N} = 8$ supergravity*, *JHEP* **03** (2019) 115, [[arXiv:1901.05932](#)].
- [13] S. Abreu, L. J. Dixon, E. Herrmann, B. Page, and M. Zeng, *The two-loop five-point amplitude in $\mathcal{N} = 8$ supergravity*, *JHEP* **03** (2019) 123, [[arXiv:1901.08563](#)].
- [14] S. Abreu, J. Dormans, F. Febres Cordero, H. Ita, B. Page, and V. Sotnikov, *Analytic Form of the Planar Two-Loop Five-Parton Scattering Amplitudes in QCD*, *JHEP* **05** (2019) 084, [[arXiv:1904.00945](#)].
- [15] H. B. Hartanto, S. Badger, C. Brnnum-Hansen, and T. Peraro, *A numerical evaluation of planar two-loop helicity amplitudes for a W-boson plus four partons*, [arXiv:1906.11862](#).
- [16] Y. Zhang, *Integrand-Level Reduction of Loop Amplitudes by Computational Algebraic Geometry Methods*, *JHEP* **09** (2012) 042, [[arXiv:1205.5707](#)].
- [17] P. Mastrolia, E. Mirabella, G. Ossola, and T. Peraro, *Scattering Amplitudes from Multivariate Polynomial Division*, *Phys. Lett.* **B718** (2012) 173–177, [[arXiv:1205.7087](#)].
- [18] J. M. Henn, *Multiloop integrals in dimensional regularization made simple*, *Phys. Rev. Lett.* **110** (2013) 251601, [[arXiv:1304.1806](#)].
- [19] J. M. Henn, *Lectures on differential equations for Feynman integrals*, *J. Phys.* **A48** (2015) 153001, [[arXiv:1412.2296](#)].
- [20] H. Ita, *Two-loop Integrand Decomposition into Master Integrals and Surface Terms*, *Phys. Rev.* **D94** (2016), no. 11 116015, [[arXiv:1510.05626](#)].
- [21] S. Abreu, F. Febres Cordero, H. Ita, M. Jaquier, B. Page, and M. Zeng, *Two-Loop Four-Gluon Amplitudes from Numerical Unitarity*, *Phys. Rev. Lett.* **119** (2017), no. 14 142001, [[arXiv:1703.05273](#)].
- [22] L. J. Dixon, J. M. Drummond, and J. M. Henn, *Bootstrapping the three-loop hexagon*, *JHEP* **11** (2011) 023, [[arXiv:1108.4461](#)].
- [23] L. J. Dixon, J. M. Drummond, M. von Hippel, and J. Pennington, *Hexagon functions and the three-loop remainder function*, *JHEP* **12** (2013) 049, [[arXiv:1308.2276](#)].

- [24] L. J. Dixon and M. von Hippel, *Bootstrapping an NMHV amplitude through three loops*, *JHEP* **10** (2014) 065, [[arXiv:1408.1505](#)].
- [25] S. Caron-Huot, L. J. Dixon, A. McLeod, and M. von Hippel, *Bootstrapping a Five-Loop Amplitude Using Steinmann Relations*, *Phys. Rev. Lett.* **117** (2016), no. 24 241601, [[arXiv:1609.00669](#)].
- [26] L. J. Dixon, M. von Hippel, and A. J. McLeod, *The four-loop six-gluon NMHV ratio function*, *JHEP* **01** (2016) 053, [[arXiv:1509.08127](#)].
- [27] L. J. Dixon, J. Drummond, T. Harrington, A. J. McLeod, G. Papathanasiou, and M. Spradlin, *Heptagons from the Steinmann Cluster Bootstrap*, *JHEP* **02** (2017) 137, [[arXiv:1612.08976](#)].
- [28] D. Chicherin, J. Henn, and V. Mitev, *Bootstrapping pentagon functions*, *JHEP* **05** (2018) 164, [[arXiv:1712.09610](#)].
- [29] S. Caron-Huot, L. J. Dixon, F. Dulat, M. von Hippel, A. J. McLeod, and G. Papathanasiou, *Six-Gluon Amplitudes in Planar $\mathcal{N} = 4$ Super-Yang-Mills Theory at Six and Seven Loops*, [[arXiv:1903.10890](#)].
- [30] A. von Manteuffel and R. M. Schabinger, *A novel approach to integration by parts reduction*, *Phys. Lett.* **B744** (2015) 101–104, [[arXiv:1406.4513](#)].
- [31] T. Peraro, *Scattering amplitudes over finite fields and multivariate functional reconstruction*, *JHEP* **12** (2016) 030, [[arXiv:1608.01902](#)].
- [32] T. Peraro, *FiniteFlow: multivariate functional reconstruction using finite fields and dataflow graphs*, *JHEP* **07** (2019) 031, [[arXiv:1905.08019](#)].
- [33] K. Chetyrkin and F. Tkachov, *Integration by parts: The algorithm to calculate ϵ -functions in 4 loops*, *Nuclear Physics B* **192** (1981), no. 1 159 – 204.
- [34] S. Laporta, *High precision calculation of multiloop Feynman integrals by difference equations*, *Int. J. Mod. Phys.* **A15** (2000) 5087–5159, [[hep-ph/0102033](#)].
- [35] A. V. Smirnov, *Algorithm FIRE – Feynman Integral REduction*, *JHEP* **10** (2008) 107, [[arXiv:0807.3243](#)].
- [36] A. V. Smirnov, *FIRE5: a C++ implementation of Feynman Integral REduction*, *Comput. Phys. Commun.* **189** (2015) 182–191, [[arXiv:1408.2372](#)].
- [37] A. V. Smirnov and F. S. Chuharev, *FIRE6: Feynman Integral REduction with Modular Arithmetic*, [[arXiv:1901.07808](#)].
- [38] P. Maierhoefer, J. Usovitsch, and P. Uwer, *Kira - A Feynman Integral Reduction Program*, *Comput. Phys. Commun.* **230** (2018) 99–112, [[arXiv:1705.05610](#)].
- [39] P. Maierhofer and J. Usovitsch, *Kira 1.2 Release Notes*, [[arXiv:1812.01491](#)].
- [40] A. von Manteuffel and C. Studerus, *Reduze 2 - Distributed Feynman Integral Reduction*, [[arXiv:1201.4330](#)].
- [41] J. Gluza, K. Kajda, and D. A. Kosower, *Towards a Basis for Planar Two-Loop Integrals*, *Phys.Rev.* **D83** (2011) 045012, [[arXiv:1009.0472](#)].
- [42] R. M. Schabinger, *A New Algorithm For The Generation Of Unitarity-Compatible Integration By Parts Relations*, *JHEP* **01** (2012) 077, [[arXiv:1111.4220](#)].
- [43] K. J. Larsen and Y. Zhang, *Integration-by-parts reductions from unitarity cuts and algebraic*

- geometry*, *Phys. Rev.* **D93** (2016), no. 4 041701, [[arXiv:1511.01071](#)].
- [44] Z. Bern, M. Enciso, H. Ita, and M. Zeng, *Dual Conformal Symmetry, Integration-by-Parts Reduction, Differential Equations and the Nonplanar Sector*, *Phys. Rev.* **D96** (2017), no. 9 096017, [[arXiv:1709.06055](#)].
- [45] R. N. Lee and A. A. Pomeransky, *Critical points and number of master integrals*, *JHEP* **11** (2013) 165, [[arXiv:1308.6676](#)].
- [46] A. Georgoudis, K. J. Larsen, and Y. Zhang, *Azurite: An algebraic geometry based package for finding bases of loop integrals*, *Comput. Phys. Commun.* **221** (2017) 203–215, [[arXiv:1612.04252](#)].
- [47] T. Bitoun, C. Bogner, R. P. Klausen, and E. Panzer, *Feynman integral relations from parametric annihilators*, [arXiv:1712.09215](#).
- [48] H. A. Chawdhry, M. A. Lim, and A. Mitov, *Two-loop five-point massless QCD amplitudes within the IBP approach*, [arXiv:1805.09182](#).
- [49] S. Badger, D. Chicherin, T. Gehrmann, G. Heinrich, J. M. Henn, T. Peraro, P. Wasser, Y. Zhang, and S. Zoia, *Analytic form of the full two-loop five-gluon all-plus helicity amplitude*, [arXiv:1905.03733](#).
- [50] D. A. Kosower, *Direct Solution of Integration-by-Parts Systems*, *Phys. Rev.* **D98** (2018), no. 2 025008, [[arXiv:1804.00131](#)].
- [51] P. Mastrolia and S. Mizera, *Feynman Integrals and Intersection Theory*, *JHEP* **02** (2019) 139, [[arXiv:1810.03818](#)].
- [52] H. Frellesvig, F. Gasparotto, S. Laporta, M. K. Mandal, P. Mastrolia, L. Mattiazzi, and S. Mizera, *Decomposition of Feynman Integrals on the Maximal Cut by Intersection Numbers*, *JHEP* **05** (2019) 153, [[arXiv:1901.11510](#)].
- [53] H. Frellesvig, F. Gasparotto, M. K. Mandal, P. Mastrolia, L. Mattiazzi, and S. Mizera, *Vector Space of Feynman Integrals and Multivariate Intersection Numbers*, [arXiv:1907.02000](#).
- [54] X. Liu and Y.-Q. Ma, *Determining arbitrary Feynman integrals by vacuum integrals*, *Phys. Rev.* **D99** (2019), no. 7 071501, [[arXiv:1801.10523](#)].
- [55] X. Liu, Y.-Q. Ma, and C.-Y. Wang, *A Systematic and Efficient Method to Compute Multi-loop Master Integrals*, *Phys. Lett.* **B779** (2018) 353–357, [[arXiv:1711.09572](#)].
- [56] Y. Wang, Z. Li, and N. Ul Basat, *Direct Reduction of Amplitude*, [arXiv:1901.09390](#).
- [57] A. Kardos, *A new reduction strategy for special negative sectors of planar two-loop integrals without Laporta algorithm*, [arXiv:1812.05622](#).
- [58] J. Böhm, A. Georgoudis, K. J. Larsen, H. Schönemann, and Y. Zhang, *Complete integration-by-parts reductions of the non-planar hexagon-box via module intersections*, *JHEP* **09** (2018) 024, [[arXiv:1805.01873](#)].
- [59] J. Böhm, A. Georgoudis, K. J. Larsen, M. Schulze, and Y. Zhang, *Complete sets of logarithmic vector fields for integration-by-parts identities of Feynman integrals*, *Phys. Rev.* **D98** (2018), no. 2 025023, [[arXiv:1712.09737](#)].
- [60] W. Decker, G.-M. Greuel, G. Pfister, and H. Schönemann, “SINGULAR 4-1-1 — A computer algebra system for polynomial computations.” <http://www.singular.uni-kl.de>, 2018.
- [61] F.-J. Pfreundt and M. Rahn, *GPI-Space*, 2018. Fraunhofer ITWM Kaiserslautern,

<http://www.gpi-space.de/>.

- [62] P. Wasser, *Analytic properties of Feynman integrals for scattering amplitudes*, M.Sc. (2016) [https://publications.ub.uni-mainz.de/theses/frontdoor.php?source_opus=100001967].
- [63] P. A. Baikov, *Explicit solutions of the three loop vacuum integral recurrence relations*, *Phys. Lett.* **B385** (1996) 404–410, [[hep-ph/9603267](https://arxiv.org/abs/hep-ph/9603267)].
- [64] R. N. Lee, *Modern techniques of multiloop calculations*, in *Proceedings, 49th Rencontres de Moriond on QCD and High Energy Interactions: La Thuile, Italy, March 22-29, 2014*, pp. 297–300, 2014. [arXiv:1405.5616](https://arxiv.org/abs/1405.5616).
- [65] Y. Zhang, *Lecture Notes on Multi-loop Integral Reduction and Applied Algebraic Geometry*, 2016. [arXiv:1612.02249](https://arxiv.org/abs/1612.02249).
- [66] The_SpaSM_group, *SpaSM: a Sparse direct Solver Modulo p*, v1.2 ed., 2017. <http://github.com/cbouilla/spasm>.
- [67] J. Böhm, W. Decker, A. Frübis-Krüger, F.-J. Pfreundt, M. Rahn, and L. Ristau, *Towards massively parallel computations in algebraic geometry*, [arXiv:1808.09727](https://arxiv.org/abs/1808.09727).
- [68] C. Jordan, M. Joswig, and L. Kastner, *Parallel enumeration of triangulations*, *Electron. J. Combin.* **25** (2018), no. 3 Paper 3.6, 27.
- [69] L. Ristau, *Using Petri nets to parallelize algebraic algorithms*, 2019. Ph.D. Thesis.
- [70] C. Reinbold, *Computation of the GIT-fan using a massively parallel implementation*, 2018. Master’s Thesis.
- [71] D. Bendle, *Massively parallel computation of tropical varieties*, 2018. Bachelor’s Thesis.
- [72] Z. Bern, E. Herrmann, S. Litsey, J. Stankowicz, and J. Trnka, *Logarithmic Singularities and Maximally Supersymmetric Amplitudes*, *JHEP* **06** (2015) 202, [[arXiv:1412.8584](https://arxiv.org/abs/1412.8584)].
- [73] N. Arkani-Hamed, J. L. Bourjaily, F. Cachazo, and J. Trnka, *Local Integrals for Planar Scattering Amplitudes*, *JHEP* **06** (2012) 125, [[arXiv:1012.6032](https://arxiv.org/abs/1012.6032)].
- [74] D. Chicherin, T. Gehrmann, J. M. Henn, N. A. Lo Presti, V. Mitev, and P. Wasser, *Analytic result for the nonplanar hexa-box integrals*, *JHEP* **03** (2019) 042, [[arXiv:1809.06240](https://arxiv.org/abs/1809.06240)].
- [75] D. Chicherin, T. Gehrmann, J. M. Henn, P. Wasser, Y. Zhang, and S. Zoia, *All master integrals for three-jet production at NNLO*, *Phys. Rev. Lett.* **123** (2019), no. 4 041603, [[arXiv:1812.11160](https://arxiv.org/abs/1812.11160)].
- [76] J. Lykke Jacobsen, Y. Jiang, and Y. Zhang, *Torus partition function of the six-vertex model from algebraic geometry*, *JHEP* **03** (2019) 152, [[arXiv:1812.00447](https://arxiv.org/abs/1812.00447)].
- [77] Y. Jiang and Y. Zhang, *Algebraic geometry and Bethe ansatz. Part I. The quotient ring for BAE*, *JHEP* **03** (2018) 087, [[arXiv:1710.04693](https://arxiv.org/abs/1710.04693)].
- [78] R. Zippel, *Probabilistic algorithms for sparse polynomials*, vol. 72, pp. 216–226, 01, 1979.
- [79] M. Ben and P. Tiwari, *A deterministic algorithm for sparse multivariate polynomial interpolation*, *Proceedings of the 20th Annual STOC* (01, 1988).
- [80] E. Kaltofen, W.-s. Lee, and A. Lobo, *Early termination in ben-or/tiwari sparse interpolation and a hybrid of zippel’s algorithm**, *Proceedings of the International Symposium on Symbolic and Algebraic Computation, ISSAC* (05, 2001).